Acta Biomaterialia 14 (2015) 197–207

Contents lists available at ScienceDirect

Acta Biomaterialia

journal homepage: www.elsevier.com/locate/actabiomat

Multifunctional calcium phosphate nanoparticles for combining near-infrared fluorescence imaging and photodynamic therapy

Katja Haedicke [a], Diana Kozlova [b], Susanna Gräfe [c], Ulf Teichgräber [a], Matthias Epple [b,*], Ingrid Hilger [a,*]

[a] Department of Experimental Radiology, Institute of Diagnostic and Interventional Radiology, Jena University Hospital, Friedrich-Schiller University Jena, 07747 Jena, Germany
[b] Inorganic Chemistry and Center for Nanointegration Duisburg-Essen (CeNIDE), University of Duisburg-Essen, 45117 Essen, Germany
[c] Biolitec Research GmbH, Research & Development, 07745 Jena, Germany

ARTICLE INFO

Article history:
Received 29 August 2014
Received in revised form 20 November 2014
Accepted 14 December 2014
Available online 19 December 2014

Keywords:
Calcium phosphate nanoparticles
Photodynamic therapy
NIRF optical imaging
Apoptosis
Vascularization

ABSTRACT

Photodynamic therapy (PDT) of tumors causes skin photosensitivity as a result of unspecific accumulation behavior of the photosensitizers. PDT of tumors was improved by calcium phosphate nanoparticles conjugated with (i) Temoporfin as a photosensitizer, (ii) the RGDfK peptide for favored tumor targeting and (iii) the fluorescent dye molecule DY682-NHS for enabling near-infrared fluorescence (NIRF) optical imaging in vivo. The nanoparticles were characterized with regard to size, spectroscopic properties and uptake into CAL-27 cells. The nanoparticles had a hydrodynamic diameter of approximately 200 nm and a zeta potential of around +22 mV. Their biodistribution at 24 h after injection was investigated via NIRF optical imaging. After treating tumor-bearing CAL-27 mice with nanoparticle-PDT, the therapeutic efficacy was assessed by a fluorescent DY-734-annexin V probe at 2 days and 2 weeks after treatment to detect apoptosis. Additionally, the contrast agent IRDye® 800CW RGD was used to assess tumor vascularization (up to 4 weeks after PDT). After nanoparticle-PDT in mice, apoptosis in the tumor was detected after 2 days. Decreases in tumor vascularization and tumor volume were detected in the next few days. Calcium phosphate nanoparticles can be used as multifunctional tools for NIRF optical imaging, PDT and tumor targeting as they exhibited a high therapeutic efficacy, being capable of inducing apoptosis and destroying tumor vascularization.

1. Introduction

Photodynamic therapy (PDT) is a promising tumor treatment modality, which allows the local generation of reactive oxygen species by selective activation of a photosensitizing agent via visible laser light [1]. Thus, the specific destruction of tumor tissue with simultaneous preservation of the healthy surrounding tissue is guaranteed. Successful treatments have already been realized with the photosensitizer Temoporfin (mTHPC), which is used as the liposomal formulation Foscan® [2,3] in clinics. Despite these observations, these and most other photosensitizers do not show any target-specific binding in tumors. Therefore, after systemic administration of the agents, the whole body and especially the skin exhibit a high photosensitivity, such that patients have to avoid direct contact with light [4,5]. Hence, it is of great interest to develop photosensitizers that show precise enrichment in tumors but not in other regions of the body [6,7].

One rising field in this regard is the use of multifunctional nanoparticulate carrier systems, which enable the loading of a photosensitizer together with other components that enhance the specificity and imaging qualities of the carriers [8–10]. These features make a combination of diagnostic imaging, drug delivery and therapy [11–14] feasible. Concerning cell-specific targeting, the conjugation of functionalized nanoparticles with receptor-binding molecules can selectively increase their uptake by target cells [15]. Various targeting moieties, such as antibodies, aptamers or small molecules, have already been used [16]. Among them, RGD peptides are particularly suitable for enhancing intratumoral probe enrichment. RGD peptides specifically bind to $\alpha_v\beta_3$ integrins on the activated endothelium of angiogenic blood vessels, they can easily be conjugated to nanoparticles and they are cheaper than antibodies [17–20].

To track the nanoparticles in vivo, near-infrared fluorescence (NIRF) optical imaging in the range of 650–900 nm [21] is an appropriate technology due to its low autofluorescence and the high penetration depth of the NIR light. Interestingly, the use of

* Corresponding authors. Tel.: +49 201 1832402; fax: +49 201 1832621 (M. Epple). Tel.: +49 3641 9325921; fax: +49 3641 9325922 (I. Hilger).
E-mail addresses: matthias.epple@uni-due.de (M. Epple), Ingrid.Hilger@med.uni-jena.de (I. Hilger).

http://dx.doi.org/10.1016/j.actbio.2014.12.009
1742-7061/

nanoparticles as carrier systems for NIRF-emitting dyes was shown to improve their admission, prolong their circulation time in the body, intensify their fluorescence and improve their photostability [22–24].

Among the different nanoparticle varieties currently available, calcium phosphate nanoparticles are very attractive [25–31] as they exhibit high biocompatibility, small size, low toxicity, high biodegradability, easy preparation and suitability for functionalization [32]. In particular, the attachment of an antibody or dye to calcium phosphate nanoparticles has shown the potential for cell-specific targeting or diagnostic fluorescence imaging [33–35]. Also, the utilization of these nanoparticles for PDT has already been demonstrated [36–38]. However, calcium phosphate nanoparticles have never hitherto been synthesized that can unite all of these aspects – NIRF optical imaging, favored tumor targeting and PDT – at once.

In this study, we designed multifunctional calcium phosphate nanoparticles made up of a calcium phosphate core as the carrier, an NIRF dye as an imaging tool, enabling localization in the body, the photosensitizer mTHPC as the drug for the PDT of tumors, and finally the RGDfK peptide for specifying delivery to endothelial cells in tumors, thus causing less skin photosensitivity compared to free mTHPC. Furthermore, the suggested nanoparticles should prospectively allow a reduction in the hydrophobicity of mTHPC. Our multifunctional nanoparticles will be shown to be suitable for PDT. In this context, the nanoparticles will be first characterized regarding size, spectroscopic properties and internalization into tumor cells in vitro. As a precondition for PDT in vivo, intratumoral enrichment will be assessed with simultaneous verification of their suitability for in vivo NIRF optical imaging. Finally, the potential of the nanoparticles for inducing apoptosis and destroying tumor vascularization after PDT will be analyzed in mice xenografts. Here we use a self-designed annexin V probe that addresses phosphatidylserine on apoptotic tumor cells, together with an integrin-targeting RGD-probe for detecting tumor vascularization.

2. Materials and methods

2.1. Cell line and animals

For in vitro experiments and as xenografts, CAL-27 cells (tongue–squamous epithelium carcinoma cells, DSMZ, Braunschweig, Germany) were used. They were cultured in Dulbecco's modified Eagle's medium (GlutaMAX™, Gibco®, Darmstadt, Germany) supplemented with 10% fetal calf serum at 37 °C in a 5% CO_2 humidified atmosphere.

For in vivo experiments, female athymic nude mice (Hsd:Athymic Nude-Foxn1^{nu} (nu/nu), Harlan Laboratories GmbH, Venray, The Netherlands) of approximately 20–25 g body weight were housed with food and water ad libitum under standard conditions. For generating xenografts, 2×10^6 CAL-27 cells in Matrigel™ (BD, Heidelberg, Germany) were implanted subcutaneously into the posterior back of mice aged 8–12 weeks and grown until they reached a diameter of approximately 5 mm. All experiments were carried out with isofluorane-anesthetized (Actavis, Munich, Germany) animals and with the approval of the regional animal committee, as well as in accordance with international guidelines on the ethical use of animals.

2.2. Preparation of multifunctional calcium phosphate nanoparticles

Silica-modified calcium phosphate nanoparticles with an inner shell of the stabilizing polymer polyethylenimine (PEI) were synthesized as described previously [34]. The preparation pathway is shown schematically in Fig. 1. After modification with a silica shell, the nanoparticles were dye-labeled to enable NIRF optical imaging by adding 200 µl of DY682-N-hydroxysuccinimidyl ester in dimethylsulfoxide (DY682-NHS, 1 mg ml^{-1}, absorption: 690 nm, emission: 709 nm, Dyomics GmbH) to 10 ml of the CaP/PEI/SiO_2 dispersion under stirring, followed by stirring for 30 min at room temperature. For the functionalization with thiol groups, the DY682-labeled nanoparticle dispersion was added to a mixture of 40 ml of ethanol and 50 µl of (3-thiolpropyl)trimethoxysilane (MPS, Sigma-Aldrich, 95%) and stirred for 8–10 h at room temperature. Then the CaP/PEI/SiO_2/DY682/SH particles were purified by ultracentrifugation and redispersed in 8 ml of water by ultrasonication. DY682-labeled thiol-terminated calcium phosphate nanoparticles were loaded with meta-tetra-hydroxyphenyl-chlorin (mTHPC; Biolitec Research GmbH) as follows: 200 µl of mTHPC in 2-propanol (1 mg ml^{-1}) was added to 8 ml of the CaP/PEI/SiO_2/DY682/SH dispersion under stirring, followed by stirring for 1 h at room temperature. The CaP/PEI/SiO_2/DY682/SH/mTHPC particles were collected by ultracentrifugation and redispersed in 8 ml of water by ultrasonication.

For covalent conjugation, 500 µl of RGDfK peptide in PBS (cyclo(-Arg-Gly-Asp-D-Phe-Lys) trifluoroacetate salt, 1 mg ml^{-1}, Bachem AG) were activated with 200 µl of the crosslinker 4-(*N*-maleimidomethyl)cyclohexane-1-carboxylic acid 3-sulpho-*N*-hydroxysuccinimide ester sodium salt (4 mM, p.a., Sigma-Aldrich) for 3–4 h at room temperature. Next, 5 ml of the CaP/PEI/SiO_2/DY682/SH/mTHPC nanoparticles were added to the activated crosslinker and peptide mixture and reacted for 24 h at 4 °C.

After the conjugation reaction, the nanoparticles were purified by centrifugation for 15 min at 14,500 *g* and redispersed in 5 ml of water (UP50H, Hielscher, Ultrasound Technology, sonotrode 2, cycle 0.8, amplitude 70%, 8 s).

For long-term storage, the dispersions were freeze-dried. For this, 15 mg of D-(+)-trehalose dihydrate (Aldrich) was added to 1 ml of the dispersion (CaP/PEI/SiO_2/DY682/SH, CaP/PEI/SiO_2/DY682/SH/mTHPC, CaP/PEI/SiO_2/DY682/SH/mTHPC-RGDfK), which was then shock-frozen with liquid nitrogen. This system was lyophilized for 48 h at 0.31 mbar and −7 °C [39].

2.3. Characterization of multifunctional calcium phosphate nanoparticles

Scanning electron microscopy (SEM) was performed with an ESEM Quanta 400 instrument with gold/palladium-sputtered samples. Dynamic light scattering (DLS) and zeta potential determinations were performed with a Zetasizer nanoseries instrument (Malvern Nano-ZS, laser: $\lambda = 532$ nm) using the Smoluchowski approximation and taking the data from the Malvern software without further correction. The particle size data refer to scattering intensity distributions (*z*-average). Ultracentrifugation was performed at 25 °C with an Optima XL-I instrument (Beckman-Coulter). Absorption spectra were recorded with a Varian Cary 300 spectrophotometer. Emission spectra were recorded with an Agilent Cary Eclipse spectrophotometer. Freeze-drying (lyophilization) was performed with a Christ, Alpha 2-4 LSC instrument.

2.4. Cellular uptake of multifunctional calcium phosphate nanoparticles

For determining the cellular uptake of the nanoparticles, CAL-27 cells were grown for 2 days in a chamber slide. They were then incubated for 24 h with 1 nmol (with respect to the dye concentration) of the nanoparticle formulation conjugated with DY682 and mTHPC (NP-DY682-mTHPC). Cell nuclei were counterstained with 2 µg ml^{-1} Hoechst-33258 (Applichem, Darmstadt, Germany). Cells were analyzed with an EVOS fluorescence microscope (AMG, Bothell, WA, USA) using a filter for Hoechst-stained cell nuclei

(extinction: 357 ± 44 nm; emission: 447 ± 60 nm) and another one for identification of the nanoparticles (extinction: 628 ± 40 nm; emission: 692 ± 40 nm).

2.5. Intratumoral enrichment and biodistribution of multifunctional calcium phosphate nanoparticles

To show the intratumoral enrichment of the three different nanoparticle formulations (NP-DY682, NP-DY682-mTHPC and NP-DY682-mTHPC-RGD) in vivo, 1 nmol (with respect to the dye concentration) of each was injected intravenously into three mice with CAL-27 tumors. The background fluorescence intensity of the animals was measured before injection (−1 h), as well as 0, 2, 4, 6, 8 and 24 h thereafter, using the Maestro™ in vivo fluorescence imaging system (excitation filter: 615–665 nm; emission filter: 700 nm longpass; Cri Inc., Woburn, MA, USA). The fluorescence contrast between tumor and muscle was calculated by subtracting the fluorescence of the muscle (an area in the neck of the mice) from that of the tumor.

To analyze the biodistribution of the nanoparticles, mice were sacrificed 24 h after injection and the fluorescence of the tumors and organs was measured ex vivo. The tumors were subsequently halved and the fluorescence intensity of the moieties was measured again.

2.6. PDT treatment with multifunctional calcium phosphate nanoparticles

Nanoparticle-PDT was carried out using the nanoparticles loaded with the dye DY682, the photosensitizer mTHPC and the RGDfK peptide (NP-DY682-mTHPC-RGD). Nanoparticles were injected intravenously into four mice with CAL-27 tumors with 100 μg of mTHPC per kg body weight. Twenty-four hours later, the tumors were illuminated with a 2 W 652 nm Ceralas PDT laser (Biolitec AG, Jena, Germany), with a power density of 0.1 W cm^{-2} and a total light dose of 100 J cm^{-2}.

2.7. Imaging of the therapeutic efficacy of nanoparticle-PDT via apoptotic tumor cells

Apoptosis after nanoparticle-PDT was imaged with DY-734-annexin V, a fluorescent probe with high affinity to phosphatidylserine on apoptotic cells, which was designed and characterized previously [40]. In short, annexin V (Abcam, Cambridge, UK) was coupled to the NIRF dye DY-734-NHS (Dyomics GmbH, Jena, Germany) by mixing both components for 2 h in coupling buffer and subsequent extraction of the probe by ultracentrifugation. The absorption spectrum of the probe was measured directly after coupling and the dye-to-protein ratio was calculated based on the Lambert–Beer law.

To detect apoptotic tumor cells in vivo, DY-734-annexin V (4 nmol per kg weight) was injected intravenously into the nanoparticle-PDT-treated mice 2 days and 2 weeks after the therapy. The fluorescence intensity of the animals was measured before injection of the probe (−1 h), as well as 0, 2, 4, 6, 8, 24 and 48 h thereafter, with the Maestro™ in vivo fluorescence imaging system (excitation filter: 670–710 nm; emission filter: 750 nm longpass). By subtracting the fluorescence of the muscle (area in the animal's neck) from that of the tumor, the fluorescence contrast from tumor to muscle was calculated. The fluorescence contrast before probe injection (−1 h) was subtracted from all other time points investigated.

2.8. Imaging of the therapeutic efficacy of nanoparticle-PDT via tumor vascularization and volume

Alterations of the tumor vascularization after nanoparticle-PDT were detected with the commercial contrast agent IRDye®800CW RGD Optical Probe (LI-COR®Biosciences, Lincoln, NE, USA), which targets $\alpha_v\beta_3$ integrins on endothelial cells in the tumor. The contrast medium (40 nmol per kg body weight) was injected intravenously into mice before as well as 1, 2 and 4 weeks after nanoparticle-PDT to detect changes in the tumor vascularization with time. Fluorescence signals of the tumors were acquired with the Maestro™ in vivo fluorescence imaging system (excitation filter: 670–710 nm; emission filter: 750 nm longpass) at 24 h after injection of the IRDye® 800CW RGD. The relative fluorescence intensity is stated with regard to the fluorescence intensity before PDT (0 weeks).

To observe tumor regression, the tumor volume was measured before treatment as well as up to 4 weeks thereafter using a digital caliper and the equation $V = \pi/6 \times (\text{length} \times \text{width} \times \text{height})$. Regarding to the volume before PDT (0 days), the relative tumor volume was calculated with time after therapy.

2.9. Biodistribution of DY-734-annexin V and IRDye® 800CW RGD

Analysis of the biodistribution of the apoptosis- and vascularization-detecting probes was carried out in animals with nanoparticle-PDT at 4 weeks after therapy and at 14 days after the last DY-734-annexin V injection or 24 h after the last injection of IRDye® 800CW RGD. Animals were sacrificed at the mentioned time points and the fluorescence signals of the tumors and organs were measured ex vivo using the Maestro™ in vivo fluorescence imaging system (excitation filter: 670–710 nm; emission filter: 750 nm longpass).

2.10. Statistical analysis

Data are given as mean ± standard deviation. The statistical significance was evaluated by Student's two-tailed *t*-test. If this test failed, a Mann–Whitney Rank Sum test was used. A *p*-value of less than 0.05 was considered statistically significant.

3. Results

3.1. In vitro characterization of multifunctional calcium phosphate nanoparticles

Calcium phosphate nanoparticles were prepared by rapid precipitation from water with the simultaneous addition of PEI to make them stable. They were then modified with a silica shell, followed by labeling with the fluorescent dye DY682. After thiol functionalization, the particles were loaded with a photosensitizer mTHPC and finally conjugated with RGDfK peptide. The preparation pathway is shown schematically in Fig. 1.

The morphology and particle size distribution of the synthesized nanoparticles were characterized by DLS and SEM. Table 1 lists the major colloidal properties of the different multifunctional calcium phosphate nanoparticle formulations.

The hydrodynamic diameters of all nanoparticle formulations as measured by DLS were around 200 nm (Fig. 2). The size distribution was relatively narrow with a polydispersity index (PDI) of 0.18–0.22. The nanoparticle surface was slightly positively charged, with a zeta potential of around +22 mV in water, due to the presence of the cationic polyelectrolyte PEI. Obviously this is not compensated by the negative charge of mTHPC.

SEM images of the nanoparticles showed a nearly spherical shape, with an average diameter of 50–100 nm (Fig. 3). The difference between the hydrodynamic diameter as determined by DLS and the diameter of the solid core as determined by SEM suggests that some agglomeration of the nanoparticles occurs in dispersion. The increasing diameter with increasing level of functionalization (Table 1) is therefore not due to an increase in primary particle size

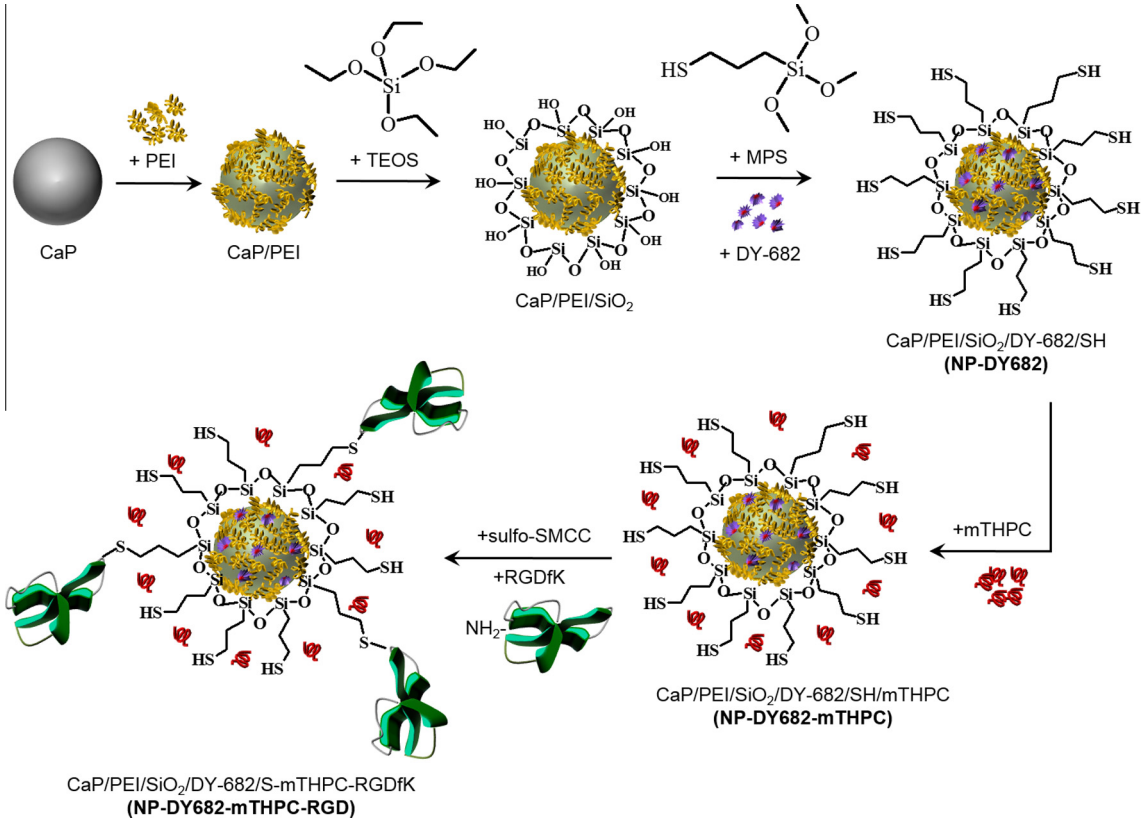

Fig. 1. Schematic representation of RGDfK-conjugated calcium phosphate nanoparticles loaded with a fluorescent dye and a photosensitizer. Silica-modified nanoparticles ($CaP/PEI/SiO_2$) were labeled with the fluorescent dye DY682-NHS (purple) and further functionalized with thiol groups ($CaP/PEI/SiO_2/DY682/SH$ = NP-DY682). Thiol-functionalized nanoparticles were additionally loaded with the photosensitizer mTHPC (red, $CaP/PEI/SiO_2/DY682/SH/mTHPC$ = NP-DY682-mTHPC) and finally conjugated with the RGDfK-peptid (green, $CaP/PEI/SiO_2/DY682/S$-mTHPC-RGDfK = NP-DY682-mTHPC-RGD).

Table 1
DLS data of water-dispersed functionalized calcium phosphate nanoparticles.

Sample	Hydrodynamic diameter (nm)	PDI	Zeta potential (mV)
NP-DY682	170 ± 99	0.182	23 ± 6
NP-DY682-mTHPC	198 ± 95	0.228	20 ± 6
NP-DY682-mTHPC-RGD	205 ± 102	0.227	24 ± 4

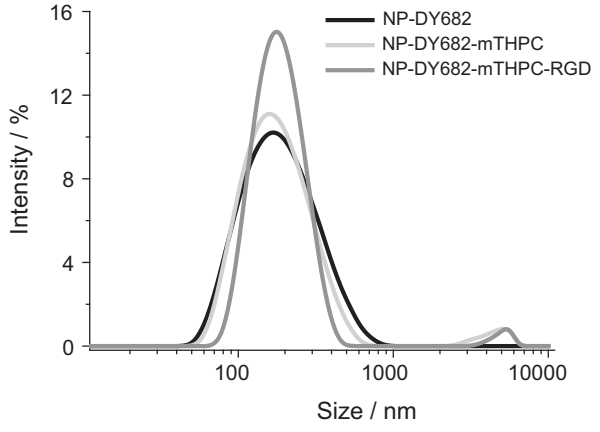

Fig. 2. DLS data (size) of three different nanoparticle formulations: NP-DY682 (black), NP-DY682-mTHPC (light gray) and NP-DY682-mTHPC-RGD (dark gray).

but to a different degree of agglomeration. This is also evident from Fig. 3, where the primary particles always have about the same diameter.

The labeling degree with DY682 as well as the loading capacity with mTHPC of the multifunctional calcium phosphate nanoparticles were determined by ultraviolet–visible spectroscopy. The concentration of DY682 in the dispersion was 5.3 μg ml^{-1} and that of calcium phosphate was 221 μg ml^{-1}, as derived from calcium concentration gleaned from atomic absorption spectroscopy and assuming the stoichiometry of hydroxyapatite, $Ca_5(PO_4)_3OH$. Taking an average particle diameter of 70 nm from the SEM data, we calculated a particle concentration of 3.9×10^{11} ml^{-1}, with about 8500 DY682 molecules incorporated into the silica shell on the surface of each particle. The loading capacity was 22.7 μg ml^{-1} for mTHPC and 37.3 μg ml^{-1} for RGDfK-conjugated and unconjugated calcium phosphate nanoparticles, respectively. The concentrations of calcium phosphate in the dispersions of conjugated and unconjugated nanoparticles were 60 and 115 μg ml^{-1}, respectively. Again taking the average particle diameter of 70 nm, the calculated particle concentrations were 1.1×10^{11} and 2.0×10^{11} ml^{-1} of RGDfK-conjugated and unconjugated calcium phosphate nanoparticles, respectively.

Note that these calculations are based on a number of assumptions, e.g. the stoichiometry of hydroxyapatite (supported at least in part by previous high-resolution transmission electron microscopy studies [41]), the density of hydroxyapatite, a spherical shape and a monodisperse particle size distribution. Obviously, these requirements are only partially fulfilled, but these assumptions are necessary to give at least an estimate of the particle concentration. We estimate the error in the particle concentrations to be about ±50%, given the limits to our knowledge about the particles, but we believe that an approximate particle concentration is a necessary requirement for assessing the particle effect in the body.

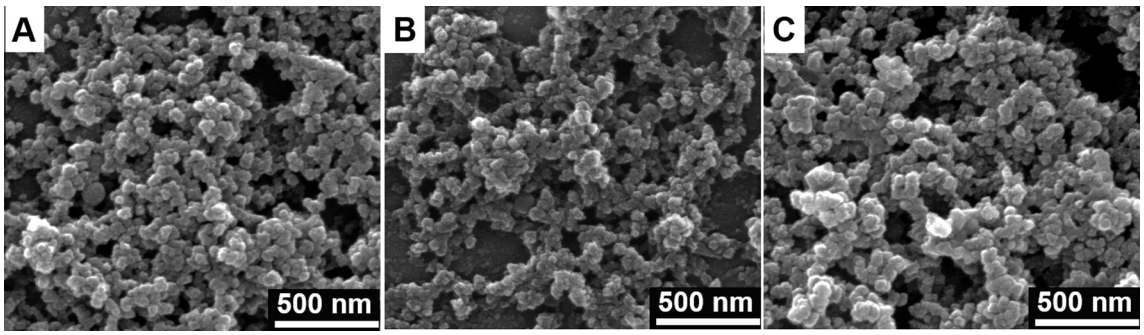

Fig. 3. Scanning electron micrographs of three different nanoparticle formulations: NP-DY682 (A), NP-DY682-mTHPC (B) and NP-DY682-mTHPC-RGD (C).

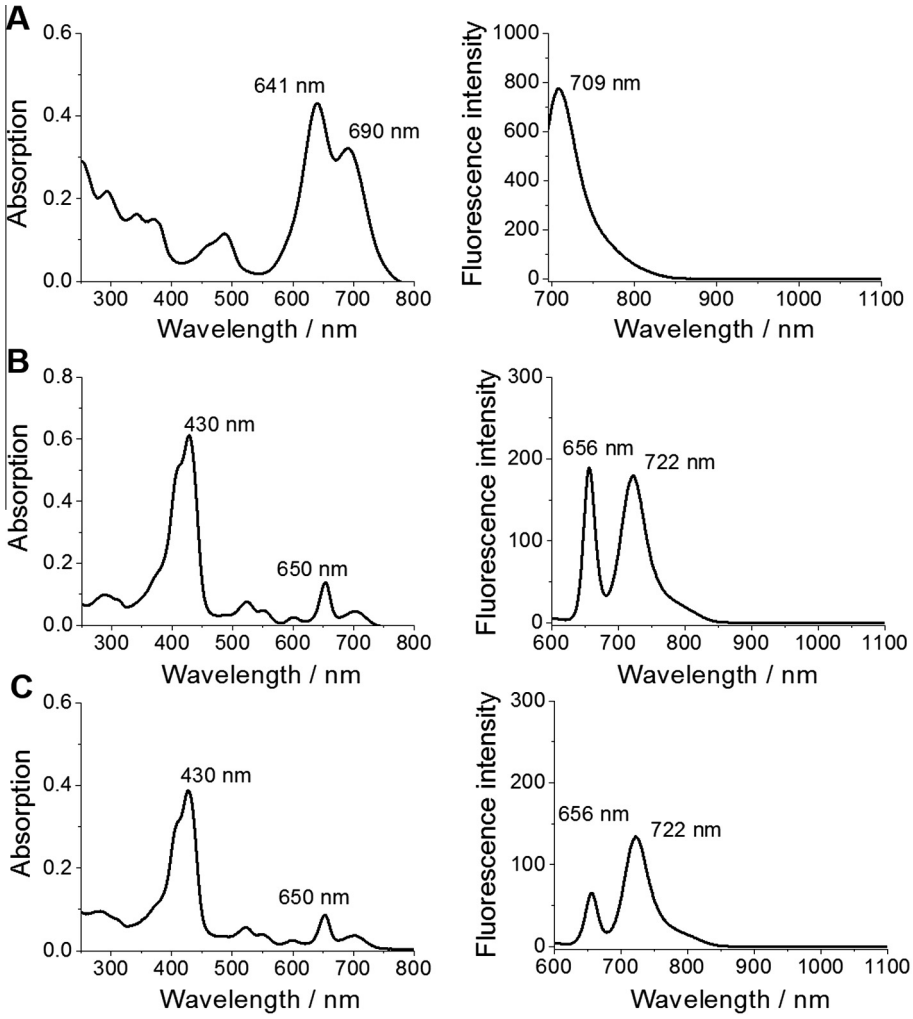

Fig. 4. Absorption (left) and fluorescence (right) spectra of NP-DY682 (A), NP-DY682-mTHPC (B) and NP-DY682-mTHPC-RGD (C) after dispersing the nanoparticles in water.

The absorption and emission spectra of the DY682-labeled nanoparticle dispersion showed split absorption bands at 641 and 690 nm and an emission band at 709 nm (Fig. 4A). No significant shift in the emission wavelength was observed in comparison to the dissolved DY682-NHS ester, suggesting that the NIRF dye remained stable after conjugation to the nanoparticles. Typical absorption spectra of NP-mTHPC and of NP-mTHPC-RGD dispersions showed a high peak at 430 nm and a smaller one at 650 nm (Fig. 4B and C, left). These spectra are similar to the absorption spectrum of dissolved mTHPC. The fluorescence spectra of NP-mTHPC and of NP-mTHPC-RGD showed two emission bands, at 656 and 722 nm (Fig. 4B and C, right). The conjugation of NP-mTHPC with the RGDfK peptide did not change the spectra noticeably. Therefore, the emission bands of the three types of functionalized nanoparticles are located in the NIRF spectral window (700–1000 nm), and their fluorescence property can be exploited for in vivo imaging.

After incubation of CAL-27 cells with the NP-DY682-mTHPC, a homogeneous fluorescence signal with enrichment in the cytoplasm of CAL-27 cells, particularly in the perinuclear region, was detected (Fig. 5). CAL-27 cells alone did not show autofluorescence.

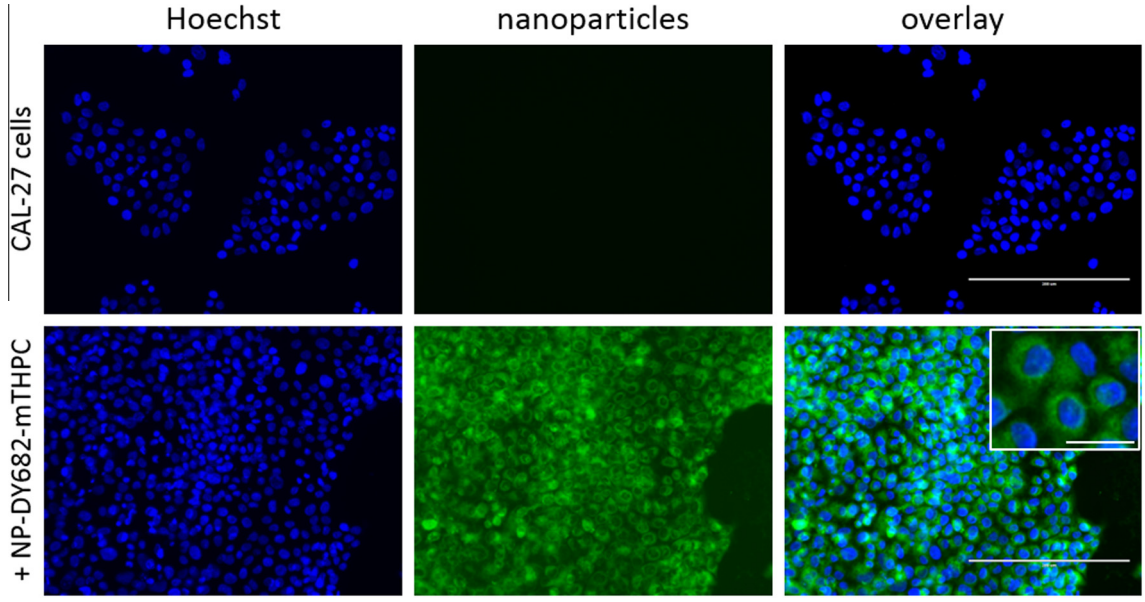

Fig. 5. Cellular uptake of NP-DY682-mTHPC in CAL-27 cells. Upper row: CAL-27 cells alone. Blue: cell nuclei stained with Hoechst. Green: nanoparticles. Bar: 200 μm (small inset: 25 μm).

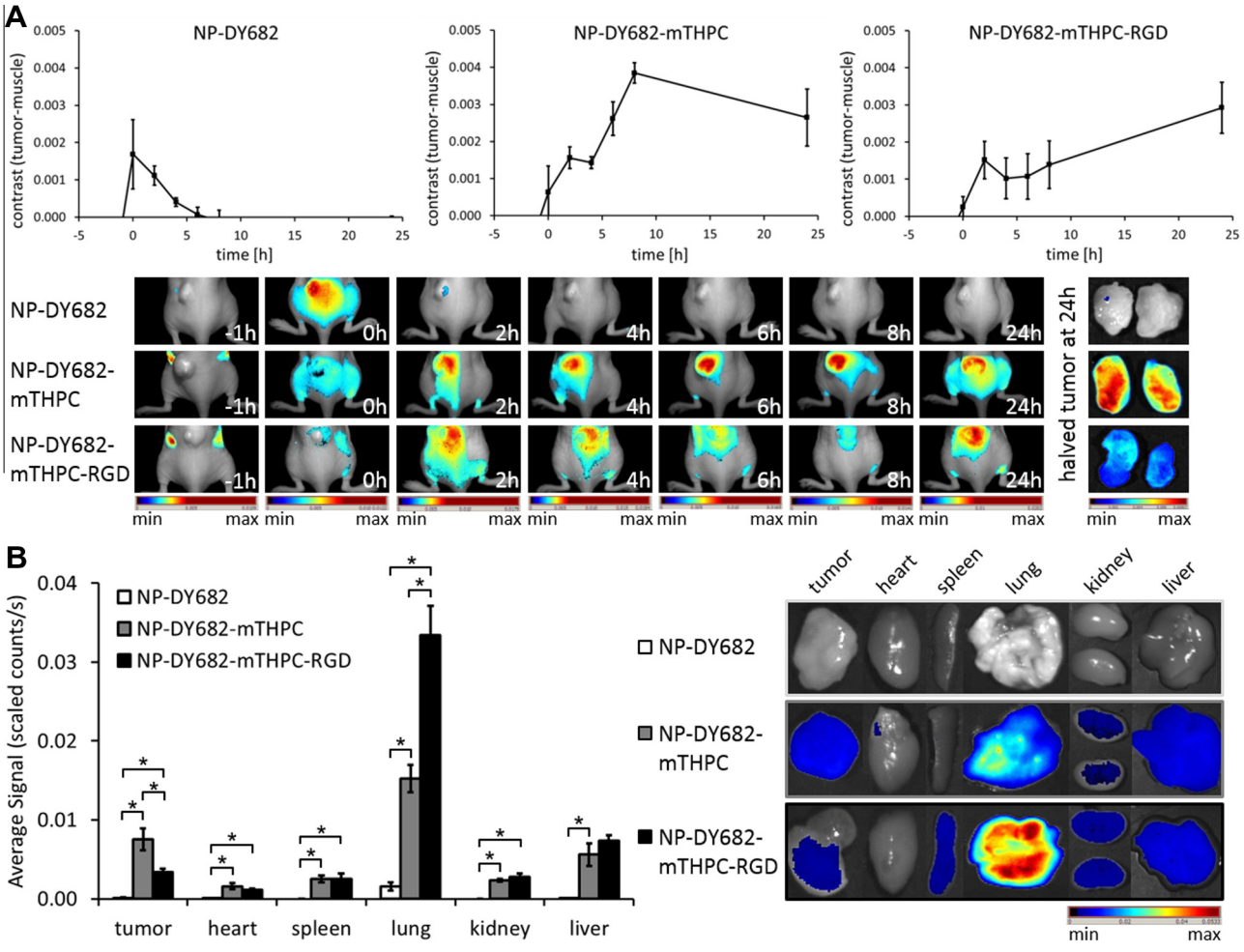

Fig. 6. Enrichment of three different formulations of nanoparticles (NP-DY682, NP-DY682-mTHPC, NP-DY682-mTHPC-RGD) in CAL-27 tumors with time and biodistribution at 24 h after application. (A) Fluorescence contrast (tumor–muscle) of NP-DY682 (left), NP-DY682-mTHPC (middle) and NP-DY682-mTHPC-RGD (right) in CAL-27 tumors up to 24 h post-injection ($n = 3$). The representative composite images illustrate the fluorescence of the nanoparticles with time after injection in mice carrying CAL-27 tumors. The composite images on the right show representative halved CAL-27 tumors at 24 h after injection of the respective nanoparticles. (B) Biodistribution of NP-DY682 (white bars), NP-DY682-mTHPC (gray bars) and NP-DY682-mTHPC-RGD (black bars) in CAL-27 tumor-bearing mice at 24 h after injection ($n = 3$, kidney $n = 6$, $^{*}p < 0.05$). Composite images show the corresponding fluorescence of the organs.

3.2. Intratumoral enrichment and biodistribution of multifunctional calcium phosphate nanoparticles

After injecting the nanoparticles into the CAL-27 tumor-bearing mice, a differing enrichment pattern in tumors with time was observed for every formulation (Fig. 6A).

While NP-DY682 showed just a low fluorescence contrast between tumor and muscle shortly after injection (0–2 h, 0.0017–0.0011 scaled counts s^{-1}) and a fast decline of the signal as little as 4 h later (0.0004 scaled counts s^{-1}), NP-DY682-mTHPC showed a sharp increase in the fluorescence contrast up to 8 h after injection (0.0038 scaled counts s^{-1}) and a small decrease up to 24 h later (0.0027 scaled counts s^{-1}). In contrast, NP-DY682-mTHPC-RGD showed a comparatively smaller increase in the fluorescence contrast up to 8 h after injection (0.0014 scaled counts s^{-1}) but a higher contrast of the tumors 24 h later (0.0029 scaled counts s^{-1}). Therefore, the highest contrast was observed at 8 h after injection with NP-DY682-mTHPC and at 24 h after injection with NP-DY682-mTHPC-RGD. The corresponding images showed the fluorescence of the nanoparticles within the mouse tumors. After sacrificing the animals and removing the tumors 24 h after injection of the nanoparticles, those enriched with NP-DY682-mTHPC showed a stronger fluorescence signal than the tumors with the two other formulations (Fig. 6A).

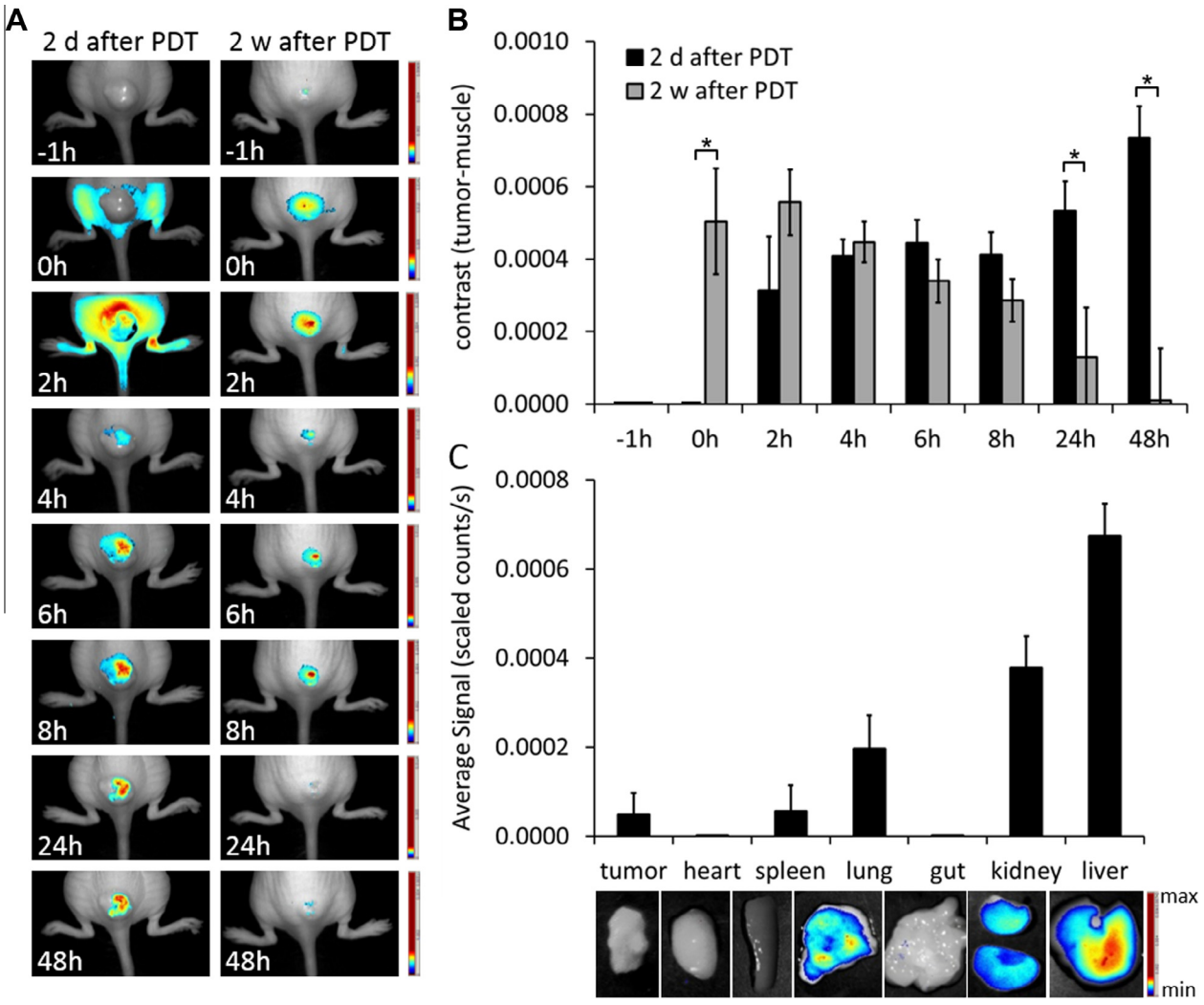

	tumor	heart	spleen	lung	gut	kidney	liver
NP	0.5 ± 0.5	0 ± 0	0.6 ± 0.6	2.0 ± 0.7	0 ± 0	3.8 ± 0.7	6.7 ± 0.7
Foslip®	1.6 ± 1.5	0 ± 0	0 ± 0	0 ± 0	0.4 ± 0.3	4.0 ± 0.8	8.7 ± 2.8
non-PDT	0.6 ± 0.6	0 ± 0	0 ± 0	0 ± 0	0.3 ± 0.3	7.9 ± 1.4	19.9 ± 5.3

Fig. 7. Detection of the therapeutic efficacy of PDT by NIRF optical imaging of apoptotic tumor cells at 2 days and 2 weeks after PDT using nanoparticles (NP-DY682-mTHPC-RGD), and the biodistribution of the DY-734-annexin V probe. (A) Representative composite images showing the fluorescence of DY-734-annexin V in CAL-27 tumor-bearing mice at 2 days (left) and 2 weeks (right) after nanoparticle-PDT. (B) Fluorescence contrast (tumor–muscle) of the DY-734-annexin V probe at 2 days (black) and 2 weeks (gray) after nanoparticle-PDT up to 48 h post-injection in mice with CAL-27 tumors ($n = 4$, $^*p < 0.05$). (C) Biodistribution of DY-734-annexin V in CAL-27 tumor-bearing mice treated with nanoparticle-PDT at 4 weeks after therapy and 14 days after the last probe injection ($n = 4$, kidney $n = 8$). The composite images show the corresponding fluorescence of the organs. The table shows the fluorescence signals ± standard error (scaled counts $s^{-1} \times 10{,}000$) of DY-734-annexin V at 4 weeks after nanoparticle-PDT (NP) and at 3 weeks after PDT with the photosensitizer formulation Foslip® and without PDT. The data of the Foslip®-PDT and non-PDT animals were taken from Ref. [40].

Regarding the biodistribution of the nanoparticles 24 h after application, for all three formulations, the strongest fluorescence signal was observed in the lung of the animals, indicating a strong accumulation of the nanoparticles within this organ (Fig. 6B). Here, a more than twofold stronger signal could be detected for NP-DY682-mTHPC-RGD (0.0334 scaled counts s^{-1}) compared to NP-DY682-mTHPC (0.0152 scaled counts s^{-1}). The weakest signal was visible after injection of NP-DY682 (0.0016 scaled counts s^{-1}). The strongest fluorescence within the tumors was found after injection of NP-DY682-mTHPC (0.0075 scaled counts s^{-1}), a weaker signal after NP-DY682-mTHPC-RGD injection (0.0034 scaled counts s^{-1}) and nearly no fluorescence at all after application of NP-DY682 (0.0001 scaled counts s^{-1}). The other organs of the animals injected with NP-DY682 also showed almost no fluorescence. After injection of NP-DY682-mTHPC or NP-DY682-mTHPC-RGD, the fluorescence in the heart, spleen, kidney and liver was almost the same for both formulations, but with weaker signals in the heart, spleen and kidney compared to the liver.

3.3. PDT with multifunctional calcium phosphate nanoparticles induces apoptosis in tumors

Apoptotic tumor cells could be imaged at 2 days after nanoparticle-PDT using the DY-734-annexin V probe, which showed increasing fluorescence in the tumors up to 48 h after injection (Fig. 7A).

In contrast, at 2 weeks after nanoparticle-PDT the fluorescence of the probe had decreased within the tumors, showing a decrease in intensity with time after injection, whereby after 24 and 48 h nearly no fluorescence could be detected anymore.

The corresponding semi-quantitative evaluation of the fluorescence intensities at 2 days after PDT showed a constant increase in the fluorescence contrast of DY-734-annexin V between tumor and muscle with time after injection, particularly from 2 to 48 h, while at 2 weeks after therapy the contrast decreased with time after probe injection (Fig. 7B). Especially from 6 to 48 h after injection, the fluorescence contrast was higher in tumors at 2 days after PDT in comparison to 2 weeks later. The significantly greater enrichment of DY-734-annexin V at 2 days after treatment at 24 and 48 h after injection indicated a specific accumulation of the probe within the tumors at these time points.

The biodistribution of DY-734-annexin V at 4 weeks after nanoparticle-PDT and 14 days after the last injection of the probe showed the strongest fluorescence in the liver (0.00067 scaled counts s^{-1}) and kidney (0.00038 scaled counts s^{-1}, Fig. 7C). A significant signal of the annexin V probe could also be detected in the lung (0.00020 scaled counts s^{-1}). The tumor (0.00005 scaled counts s^{-1}) as well as the spleen (0.00006 scaled counts s^{-1}) showed weak fluorescence, whereas the heart and the gut gave virtually no signal at all.

3.4. PDT with multifunctional calcium phosphate nanoparticles destroys tumor vascularization and diminishes tumor volume

By NIRF optical imaging, a reduction in the tumor vascularization was monitored with time after nanoparticle-PDT. In comparison to tumors before therapy (0 weeks), where a homogeneous fluorescence of IRDye® 800CW RGD was detected, a reduced fluorescence signal with only single selective spots was observed thereafter, with the strongest decrease in fluorescence intensity at 1 week after treatment (Fig. 8A).

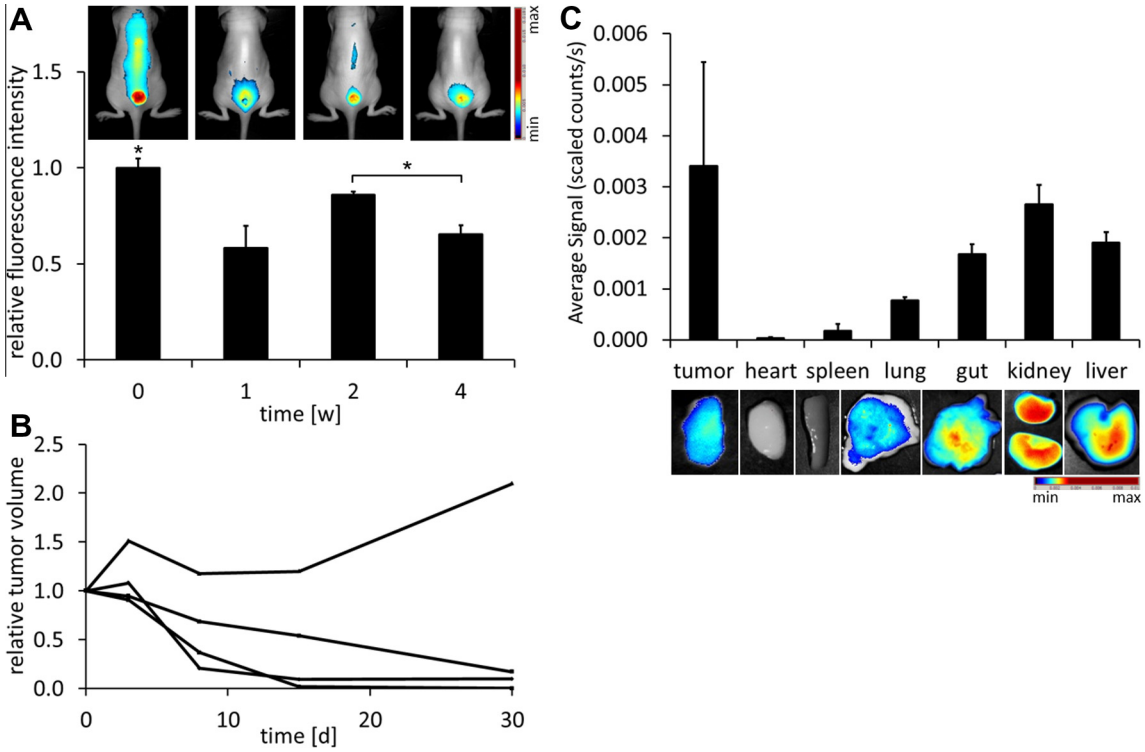

Fig. 8. Detection of the therapeutic efficacy of PDT via reduction of the tumor vascularization as well as the tumor volume after PDT using nanoparticles (NP-DY682-mTHPC-RGD) and biodistribution of IRDye® 800CW RGD. (A) Relative fluorescence intensity (related to fluorescence before PDT) of IRDye® 800CW RGD in CAL-27 tumors with time after nanoparticle-PDT ($n = 4$, $^*p < 0.05$). Representative composite images illustrate the corresponding fluorescence of IRDye® 800CW RGD in CAL-27 tumor-bearing mice before (0 weeks) as well as 1, 2 and 4 weeks after nanoparticle-PDT. (B) Relative volume of CAL-27 tumors (related to volume before PDT) in mice with time after nanoparticle-PDT ($n = 4$). (C) Biodistribution of IRDye® 800CW RGD in CAL-27 tumor-bearing mice treated with nanoparticle-PDT at 4 weeks after therapy and 24 h after the last probe injection ($n = 4$, kidney $n = 8$). Composite images show corresponding fluorescence of the organs.

At 2 weeks after PDT, the fluorescence intensity increased slightly but did not reach the starting level. The fluorescence dropped down again at 4 weeks after therapy to a value similar to that after 1 week.

Simultaneously to the decrease in the tumor vascularization, the tumor volume diminished with time after nanoparticle-PDT in three out of four animals (Fig. 8B). Increased growth of the outer tumor area was detected in one mouse at 2 weeks after therapy.

Biodistribution analysis of IRDye® 800CW RGD (showing the vascularization) at 4 weeks after nanoparticle-PDT and 24 h after the last probe injection showed the strongest fluorescence signal within the tumors (0.0034 scaled counts s^{-1}, Fig. 8C). In comparison, weaker signals could be detected in the kidney (0.0027 scaled counts s^{-1}), liver (0.0019 scaled counts s^{-1}), gut (0.0017 scaled counts s^{-1}) and lung (0.0008 scaled counts s^{-1}). Nearly no signal was emitted by the heart and spleen.

4. Discussion

By designing multifunctional calcium phosphate nanoparticles, we have established a new tool that combines PDT, favored tumor targeting and NIRF optical imaging of the nanoparticle localization. The therapeutic efficacy of the nanoparticle-PDT was detected by apoptosis markers at 2 days after PDT, and by reduction of the tumor vascularization and the tumor volume at longer time points thereafter.

Zeta potential measurements of the nanoparticles always gave a positive charge due to the presence of PEI, despite the slightly negatively charged dye mTHPC [36]. The final conjugation step with peptide also did not change the particle charge, due to the amphoteric (net charge zero) nature of the peptide [42,43].

Investigating the cellular uptake of the nanoparticles, perinuclear enrichment in CAL-27 cells was shown. The same localization was seen after incubating CAL-27 cells with the photosensitizer formulation Foslip® [40], implying that a comparable PDT effect with a destruction of tumor cells is possible by photosensitizer-loaded nanoparticles. The proven uptake of the nanoparticles into CAL-27 cells in vitro supports a real enrichment of the nanoparticles in tumor cells in vivo. The probe enrichment in CAL-27 cells and thus an initial transport and uptake of the photosensitizer into the tumor cells is a first indispensable precondition for enabling PDT with these nanoparticles.

An accumulation of calcium phosphate nanoparticles in CAL-27 tumors in vivo was demonstrated via NIRF optical imaging with time after injection, whereby different accumulation kinetics were obtained for the different nanoparticle formulations. Here, the RGD-conjugated nanoparticles showed the slowest but also the strongest enrichment at 24 h after injection, indicating a specific accumulation in comparison to the two formulations without the RGD peptide. NP-DY682 offered just a short tumoral accumulation and a fast elimination thereafter, suggesting an enrichment due to the EPR effect (enhanced permeation and retention effect). The same accumulation kinetics was shown previously for the free dye DY-754 in A431 tumors (human epidermoid carcinoma cells) [44]. Thus, despite the different size of nanoparticles and free dye, the same favorable accumulation kinetics were obtained. This observation implies that the designed nanoparticles are promising candidates for therapeutic applications. NP-DY682-mTHPC showed a stronger enrichment in tumors than NP-DY682 alone, with a maximum at 8 h after injection. Thus, the accumulation was more effective for this formulation. The different enrichment behavior appeared not to be due to different size or zeta potential, indicating that the presence of the lipophilic mTHPC plays an important role and led to a drastically enhanced enrichment of NP-DY682-mTHPC, possibly due to interaction of mTHPC with the cell membrane. NP-DY682-mTHPC-RGD gave a slower accumulation with time, with a maximum at 24 h after application. Therefore, a specific accumulation with increasing time was observed, and again this fact was not the result of a change in size or zeta potential. As was shown with the commercial contrast agent IRDye® 800CW RGD before PDT, the nanoparticles were able to access the tumor and integrins as receptors were present and accessible. As known from the IRDye® 800CW RGD, the maximum enrichment occurs at 24 h after injection. The nanoparticles with the RGD peptide showed the same maximum, suggesting that the RGD peptide bound to integrins.

Analyzing the biodistribution of the nanoparticles at 24 h after injection, the strongest signal was detected in the lungs of the animals. Because the free dye is rarely found in the lung [44,45], this is a real signal based on the nanoparticles. We assume that the strong signal in the lung is a result of the uptake of nanoparticles by cells of the mononuclear phagocyte system and transportation thereby to this organ. In a similar way, nanoparticles are accumulated in the liver or spleen, as has been shown for other nanoparticle formulations [46,47]. Another possible explanation is the aggregation of the nanoparticles within the blood as a result of electrostatic interactions between the nanoparticles and serum proteins. Extensive aggregation might ultimately lead to a transient embolism and first-pass retention in the lung capillaries [48–50]. However, to gain better insight into this enrichment pattern, particularly in the lung, and the reasons for this process, additional studies are necessary. In comparison to the lung, other organs of the animals injected with NP-DY682 showed nearly no signal at 24 h after injection. This is an indication that the nanoparticles are excreted via bile and feces. Alternatively, renal clearance by excretion via the urine is feasible, as has already been shown for similar free dye molecules, like DY-677. This dye contains three sulphonate groups, like DY682, and therefore carries a negative charge [45]. Another, less probable possibility is the detachment of the dye from the nanoparticles by degradation of the nanoparticles (e.g. after uptake into a cell and lysosomal degradation), so that only the dye is excreted. Without the fluorescent dye, the calcium phosphate nanoparticles are no longer visible in the animals. At 24 h after injection of NP-DY682-mTHPC and NP-DY682-mTHPC-RGD, a signal was also detected in the liver. This means that, after injection, the nanoparticles were removed from the blood by cells of the mononuclear phagocyte system [46,47] and transported into the liver and, to a lesser extent, into the spleen. Taken together, this biodistribution pattern implies that tumors in the liver or lung cannot be detected by our nanoparticles, but other tumors, like superficial tumors or head and neck tumors, represent a good target.

The therapeutic efficacy of NP-DY682-mTHPC-RGD was detected via induction of apoptotic tumor cells by enrichment of DY-734-annexin V at 2 days after therapy and simultaneously via a decreased fluorescence of the integrin-targeting probe IRDye® 800CW RGD in tumors after treatment, indicating destruction of the vascularization. We should mention here that necrotic cells in the tumor are also detected by the DY-734-annexin V probe because phosphatidylserine is accessible in these cells when their membrane is disrupted, though to a lesser extent than was described previously [40]. These results indicate that the multifunctional calcium phosphate nanoparticles can reach different tumoral compartments and can affect the tumor vessels as well as the tumor cells. Whether a combination of the vascular and parenchymal effects, which are both known effects of free photosensitizers like mTHPC [51–53], could increase the therapeutic efficacy for nanoparticles has yet to be investigated. The RGD peptide on our nanoparticles could serve as a targeting moiety in order to reach and eliminate the vasculature of tumors by PDT. This vascular localization could also enable the migration of the photosensitizer into the tumor cells, either together with the nanoparticles or after detachment from the nanoparticles, thus leading to cellular effects in the

tumor. We assume that mTHPC is detached from the particles after reaching the tumor and cellular uptake. Namely, it has been shown that mTHPC can be released from poly(lactide-co-glycolide) (PLGA) nanoparticles and subsequently taken up by surrounding cells [54]. However, PLGA has a different degradation behavior than calcium phosphate.

Despite the therapeutic success achieved with the nanoparticle-PDT, the outer tumor area started to grow strongly after therapy in one mouse. The same effect was detected previously after Foslip®-PDT [40]. Possible reasons for this are an inhomogeneous distribution of the photosensitizer in this case or that this tumor was not fully covered by laser illumination. This indicates that these are key parameters to be considered in PDT application.

Interestingly, after analysis of the biodistribution of DY-734-annexin V in nanoparticle-PDT-treated animals at 4 weeks after therapy and 14 days after the last probe injection, a remarkable signal was detected in the lung. In contrast, previous investigations with the photosensitizer formulation Foslip® or untreated animals did not show any signal from DY-734-annexin V in this organ, even though identical treatment parameters (intravenous injection, same laser focus) were used. In both studies the tumors were localized at the posterior back of the animals, excluding an illumination in the area of the lung. The reason for the DY-734-annexin V signal in the lung is unknown. Possible explanations are that this is an effect of the nanoparticle-based therapy, interfering with the biodistribution of the probe, or that the nanoparticles which also accumulated in the lung might affect the physiology of this organ. Therefore, it might be possible to a certain extent that apoptosis indeed occurred in the lung after local PDT of tumors located in the posterior back of the animals. Further studies are necessary to answer this question. On the other hand, the biodistribution of IRDye® 800CW RGD at 4 weeks after nanoparticle-PDT and 24 h after the last probe injection as well as the biodistribution of DY-734-annexin V in the kidney and liver showed a comparable pattern to that shown after PDT with Foslip® [40]. This indicates that the nanoparticles did not affect the biodistribution of these probes, with the exception of the lung. In this context, the strong fluorescence signals in the kidney and liver illustrate the already known excretion pathways of both probes, with faster excretion of smaller probes by the kidney and later excretion of bound larger ones by the liver because of elimination by phagocytic macrophages. Due to these biodistribution patterns, there are no signs of any potential toxicity of the nanoparticles.

In summary, our study indicates that calcium phosphate nanoparticles can be used as a multifunctional tool for NIRF optical imaging of their localization, for transporting drugs to target cells and for PDT treatment of tumors. These nanoparticles open up opportunities for combining diagnostic imaging, drug delivery and therapy. They can be used to detect superficial, head and neck or other tumors, with the exception of those in the liver and the lung. They offer several advantages: better solubility in comparison to free dye or photosensitizer, more specific tumor targeting and thus higher efficacy of PDT, reduced skin photosensitivity and the possibility of combining different functionalities, like imaging, targeting and therapy, into a single nanoparticle by a single injection.

5. Conclusion

We have designed multifunctional calcium phosphate nanoparticles which were followed in vivo after labelling with an NIRF dye and which showed antitumor activity after PDT treatment. These nanoparticles provide a promising new tool for enhancing the therapeutic efficacy in comparison to dissolved photosensitizers by simultaneous improvement and specification of the accumulation behavior. Attaching an RGD peptide onto the nanoparticle surface enables local enrichment and a reduction in such side effects as skin photosensitivity. The fluorescent dye enhances the capability of imaging of the nanoparticle localization. Altogether, with these nanoparticles combine diagnostic imaging, tumor targeting, drug delivery and therapy.

Acknowledgements

We acknowledge the Thüringer Aufbaubank (Erfurt, Germany), the graduate academy of the Friedrich-Schiller University of Jena (Jena, Germany) and the Collaborative Research Center SFB 1093 (DFG, Germany) for funding this project. We would like to thank Yvonne Ozegowski and Susann Burgold for assistance during in vivo experiments.

Appendix A. Figures with essential color discrimination

Certain figures in this article, particularly Figs. 1 and 5–8, are difficult to interpret in black and white. The full color images can be found in the on-line version, at http://dx.doi.org/10.1016/j.actbio.2014.12.009.

References

[1] Agostinis P, Berg K, Cengel KA, Foster TH, Girotti AW, Gollnick SO, et al. Photodynamic therapy of cancer: an update. CA Cancer J Clin 2011;61:250–81.
[2] Allison RR, Sibata CH. Oncologic photodynamic therapy photosensitizers: a clinical review. Photodiagnosis Photodyn Ther 2010;7:61–75.
[3] de Visscher SA, Dijkstra PU, Tan IB, Roodenburg JL, Witjes MJ. MTHPC mediated photodynamic therapy (PDT) of squamous cell carcinoma in the head and neck: a systematic review. Oral Oncol 2013;49:192–210.
[4] Mannino S, Molinari A, Sabatino G, Ciafre SA, Colone M, Maira G, et al. Intratumoral vs systemic administration of meta-tetrahydroxyphenylchlorin for photodynamic therapy of malignant gliomas: assessment of uptake and spatial distribution in C6 rat glioma model. Int J Immunopathol Pharmacol 2008;21:227–31.
[5] Shieh MJ, Peng CL, Chiang WL, Wang CH, Hsu CY, Wang SJJ, et al. Reduced skin photosensitivity with meta-tetra(hydroxyphenyl)chlorin-loaded micelles based on a poly(2-ethyl-2-oxazoline)-b-poly(D,L-lactide) diblock copolymer in vivo. Mol Pharm 2010;7:1244–53.
[6] Shirasu N, Nam SO, Kuroki M. Tumor-targeted photodynamic therapy. Anticancer Res 2013;33:2823–31.
[7] Sibani SA, McCarron PA, Woolfson AD, Donnelly RF. Photosensitiser delivery for photodynamic therapy. Part 2. Systemic carrier platforms. Expert Opin Drug Deliv 2008;5:1241–54.
[8] Jia X, Jia L. Nanoparticles improve biological functions of phthalocyanine photosensitizers used for photodynamic therapy. Curr Drug Metab 2012;13:1119–22.
[9] Tacelosky DM, Creecy AE, Shanmugavelandy SS, Smith JP, Claxton DF, Adair JH, et al. Calcium phosphosilicate nanoparticles for imaging and photodynamic therapy of cancer. Discovery Med 2012;13:275–85.
[10] Wang C, Cheng L, Liu Z. Upconversion nanoparticles for photodynamic therapy and other cancer therapeutics. Theranostics 2013;3:317–30.
[11] Park K, Lee S, Kang E, Kim K, Choi K, Kwon IC. New generation of multifunctional nanoparticles for cancer imaging and therapy. Adv Funct Mater 2009;19:1553–66.
[12] Singh AK, Hahn MA, Gutwein LG, Rule MC, Knapik JA, Moudgil BM, et al. Multi-dye theranostic nanoparticle platform for bioimaging and cancer therapy. Int J Nanomed 2012;7:2739–50.
[13] Asghari S, Johari SA, Lee JH, Kim YS, Jeon YB, Choi HJ, et al. Toxicity of various silver nanoparticles compared to silver ions in Daphnia magna. J Nanobiotechnol 2012;10:11.
[14] Huang P, Li Z, Lin J, Yang D, Gao G, Xu C, et al. Photosensitizer-conjugated magnetic nanoparticles for in vivo simultaneous magnetofluorescent imaging and targeting therapy. Biomaterials 2011;32:3447–58.
[15] Accardo A, Tesauro D, Morelli G. Peptide-based targeting strategies for simultaneous imaging and therapy with nanovectors. Polym J 2013;45:481–93.
[16] Kozlova D, Epple M. Biological targeting with nanoparticles: state of the art. BioNanoMat 2013;14:161–70.
[17] Chen H, Zhen Z, Tang W, Todd T, Chuang YJ, Wang L, et al. Label-free luminescent mesoporous silica nanoparticles for imaging and drug delivery. Theranostics 2013;3:650–7.
[18] Rangger C, Helbok A, von Guggenberg E, Sosabowski J, Radolf T, Prassl R, et al. Influence of PEGylation and RGD loading on the targeting properties of radiolabeled liposomal nanoparticles. Int J Nanomed 2012;7:5889–900.
[19] Rangger C, Helbok A, Sosabowski J, Kremser C, Koehler G, Prassl R, et al. Tumor targeting and imaging with dual peptide conjugated multifunctional liposomal nanoparticles. Int J Nanomed 2013;8:4659–71.

[20] Strijkers GJ, Kluza E, Van Tilborg GA, van der Schaft DW, Griffioen AW, Mulder WJ, et al. Paramagnetic and fluorescent liposomes for target-specific imaging and therapy of tumor angiogenesis. Angiogenesis 2010;13:161–73.
[21] Weissleder R. A clearer vision for in vivo imaging. Nat Biotechnol 2001;19:316–7.
[22] Luo S, Zhang E, Su Y, Cheng T, Shi C. A review of NIR dyes in cancer targeting and imaging. Biomaterials 2011;32:7127–38.
[23] Quek C-H, Leong KW. Near-infrared fluorescent nanoprobes for in vivo optical imaging. Nanomaterials 2012;2:92–112.
[24] Merian J, Gravier J, Navarro F, Texier I. Fluorescent nanoprobes dedicated to in vivo imaging: from preclinical validations to clinical translation. Molecules 2012;17:5564–91.
[25] Padilla Mondejar S, Kovtun A, Epple M. Lanthanide-doped calcium phosphate nanoparticles with high internal crystallinity and with a shell of DNA as fluorescent probes in cell experiments. J Mater Chem 2007;17:4153–9.
[26] Kester M, Heakal Y, Fox T, Sharma A, Robertson GP, Morgan TT, et al. Calcium phosphate nanocomposite particles for in vitro imaging and encapsulated chemotherapeutic drug delivery to cancer cells. Nano Lett 2008;8:4116–21.
[27] Guo Y, Shi D, Lian J, Dong Z, Wang W, Cho H, et al. Quantum dot conjugated hydroxylapatite nanoparticles for in vivo imaging. Nanotechnology 2008;19:175102–8.
[28] Morgan TT, Muddana HS, Altinoglu EI, Rouse SM, Tabakovic A, Tabouillot T, et al. Encapsulation of organic molecules in calcium phosphate nanocomposite particles for intracellular imaging and drug delivery. Nano Lett 2008;8:4108–15.
[29] Min KH, Lee HJ, Kim K, Kwon IC, Jeong SY, Lee SC. The tumor accumulation and therapeutic efficacy of doxorubicin carried in calcium phosphate-reinforced polymer nanoparticles. Biomaterials 2012;33:5788–97.
[30] Sokolova VV, Radtke I, Heumann R, Epple M. Effective transfection of cells with multi-shell calcium phosphate–DNA nanoparticles. Biomaterials 2006;27:3147–53.
[31] Zhang X, Kovtun A, Mendoza-Palomares C, Oulad-Abdelghani M, Facca S, Fioretti F, et al. SiRNA-loaded multi-shell nanoparticles incorporated into a multilayered film as a reservoir for gene silencing. Biomaterials 2010;31:6013–8.
[32] Epple M, Ganesan K, Heumann R, Klesing J, Kovtun A, Neumann S, et al. Application of calcium phosphate nanoparticles in biomedicine. J Mater Chem 2010;20:18–23.
[33] Altinoğlu EI. Indocyanine green-encapsulating calcium phosphosilicate nanoparticles: bifunctional theranostic vectors for near infrared diagnostic imaging and photodynamic therapy [Ph.D. thesis]. The Pennsylvania State University; 2010.
[34] Kozlova D, Chernousova S, Knuschke T, Buer J, Westendorf AM, Epple M. Cell targeting by antibody-functionalized calcium phosphate nanoparticles. J Mater Chem 2012;22:396–404.
[35] Barth BM, Sharma R, Altinoglu EI, Morgan TT, Shanmugavelandy SS, Kaiser JM, et al. Bioconjugation of calcium phosphosilicate composite nanoparticles for selective targeting of human breast and pancreatic cancers in vivo. ACS Nano 2010;4:1279–87.
[36] Klesing J, Wiehe A, Gitter B, Gräfe S, Epple M. Positively charged calcium phosphate/polymer nanoparticles for photodynamic therapy. J Mater Sci Mater Med 2010;21:887–92.
[37] Schwiertz J, Wiehe A, Gräfe S, Gitter B, Epple M. Calcium phosphate nanoparticles as efficient carriers for photodynamic therapy against cells and bacteria. Biomaterials 2009;30:3324–31.
[38] Barth BM, Altinoğlu EI, Shanmugavelandy SS, Kaiser JM, Crespo-Gonzalez D, DiVittore NA, et al. Targeted indocyanine-green-loaded calcium phosphosilicate nanoparticles for in vivo photodynamic therapy of leukemia. ACS Nano 2011;5:5325–37.
[39] Klesing J, Chernousova S, Epple M. Freeze-dried cationic calcium phosphate nanorods as versatile carriers of nucleic acids (DNA, siRNA). J Mater Chem 2012;22:199–204.
[40] Haedicke K, Grafe S, Lehmann F, Hilger I. Multiplexed in vivo fluorescence optical imaging of the therapeutic efficacy of photodynamic therapy. Biomaterials 2013;34:10075–83.
[41] Urch H, Vallet-Regi M, Ruiz L, Gonzalez-Calbet JM, Epple M. Calcium phosphate nanoparticles with adjustable dispersability and crystallinity. J Mater Chem 2009;19:2166–71.
[42] Mathews AS, Ahmad S, Shahin M, Lavasanifar A, Kaur K. Peptide modified polymeric micelles specific for breast cancer cells. Bioconjugate Chem 2013;24:560–70.
[43] Fu L, Tang J, Shi K, Chen W, Zhang Q, He Q. Dual-ligand liposomes containing RGD and TAT for enhanced cell selectivity and internalization. Asian J Pharm Sci 2012;7:225–9.
[44] Kossatz S, Behe M, Mansi R, Saur D, Czerney P, Kaiser WA, et al. Multifactorial diagnostic NIR imaging of CCK2R expressing tumors. Biomaterials 2013;34:5172–80.
[45] Hamann FM, Brehm R, Pauli J, Grabolle M, Frank W, Kaiser WA, et al. Controlled modulation of serum protein binding and biodistribution of asymmetric cyanine dyes by variation of the number of sulphonate groups. Mol Imaging 2011;10:258–69.
[46] Botella P, Abasolo I, Fernandez Y, Muniesa C, Miranda S, Quesada M, et al. Surface-modified silica nanoparticles for tumor-targeted delivery of camptothecin and its biological evaluation. J Control Release 2011;156:246–57.
[47] Martins SM, Sarmento B, Nunes C, Lucio M, Reis S, Ferreira DC. Brain targeting effect of camptothecin-loaded solid lipid nanoparticles in rat after intravenous administration. Eur J Pharm Biopharm 2013;85:488–502.
[48] Shenoy D, Little S, Langer R, Amiji M. Poly(ethylene oxide)-modified poly(beta-amino ester) nanoparticles as a pH-sensitive system for tumor-targeted delivery of hydrophobic drugs. Part 2. In vivo distribution and tumor localization studies. Pharm Res 2005;22:2107–14.
[49] Xie G, Sun J, Zhong G, Shi L, Zhang D. Biodistribution and toxicity of intravenously administered silica nanoparticles in mice. Arch Toxicol 2010;84:183–90.
[50] Zhang JS, Liu F, Huang L. Implications of pharmacokinetic behavior of lipoplex for its inflammatory toxicity. Adv Drug Deliv Rev 2005;57:689–98.
[51] Dolmans DE, Kadambi A, Hill JS, Flores KR, Gerber JN, Walker JP, et al. Targeting tumor vasculature and cancer cells in orthotopic breast tumor by fractionated photosensitizer dosing photodynamic therapy. Cancer Res 2002;62:4289–94.
[52] Garrier J, Bressenot A, Grafe S, Marchal S, Mitra S, Foster TH, et al. Compartmental targeting for mTHPC-based photodynamic treatment in vivo: correlation of efficiency, pharmacokinetics, and regional distribution of apoptosis. Int J Radiat Oncol Biol Phys 2010;78:563–71.
[53] Lassalle HP, Dumas D, Grafe S, D'Hallewin MA, Guillemin F, Bezdetnaya L. Correlation between in vivo pharmacokinetics, intratumoral distribution and photodynamic efficiency of liposomal mTHPC. J Control Release 2009;134:118–24.
[54] Low PS, Kularatne SA. Folate-targeted therapeutic and imaging agents for cancer. Curr Opin Chem Biol 2009;13:256–62.